Long-term interaction of wollastonite with acid mine water and effects on arsenic and metal removal

J.C. Fernández-Caliani [*], C. Barba-Brioso, R. Pérez-López

Departamento de Geología, Facultad de Ciencias Experimentales, Universidad de Huelva, 21071-Huelva, Spain

Abstract

This paper reports the results of a laboratory experiment conducted to investigate the effects of wollastonite dissolution on removal of potentially toxic trace elements from stream waters affected by acid mine drainage (AMD). Nearly pure wollastonite was treated with natural acid mine water (pH 2.1) for different lengths of time (15, 30, 50 and 80 days). The compositional and textural characterization of the solid reaction products suggests that wollastonite was incongruently dissolved leaving a residual amorphous silica-rich phase that preserved the prismatic morphology of the parent wollastonite. The release of Ca into solution resulted in a pH increase from 2.1 to 3.5, and subsequent precipitation of gypsum as well as poorly crystallized Fe–Al oxy-hydroxides and oxy-hydroxysulfates whose components derived from the AMD solution. A geochemical modeling approach of the wollastonite–AMD interaction using the PHREEQC code indicated supersaturation with respect to schwertmannite (saturation index = 10.7–15.7), jarosite (SI = 8.7–10.2), alunite (SI = 5.1), goethite (SI = 4.7) and jurbanite (SI = 2.2). These secondary phases developed a thin coating on the reacted wollastonite surface, readily cracked and flaked off upon drying, that acted as a sink for trace elements, especially As, Cu and Zn, as indicated by their enrichment relative to the starting wollastonite. At such low pH values, adsorption of As oxyanions on the positively charged solid particles and coprecipitation of metals (mainly Cu and Zn) with the newly formed Fe oxy-hydroxides and oxy-hydroxysulfates seem to be the dominant processes controlling the removal of trace elements.
© 2008 Elsevier Ltd. All rights reserved.

1. Introduction

Wollastonite is a natural calcium silicate $(CaSiO_3)$ that typically occurs in skarn-type deposits, inside the contact metamorphic aureoles developed in carbonate rocks by the intrusion of granitic plutons (e.g., Gerdes and Valley, 1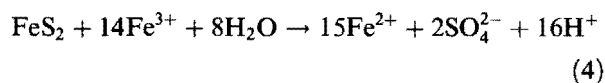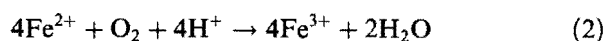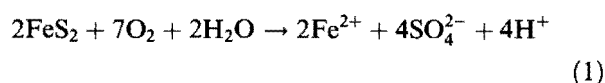994; Fernández-Caliani and Galán, 1998; Grammatiko-poulos and Clark, 2006). Traditionally it has been used for ceramic applications, such as glazes and body mixes for fast-fired wall tiles, but more recently it is being used increasingly in asbestos replacement and reinforcing filler for plastics, paints and resins, metallurgical fluxes as well as biomaterial (for artificial bone and dental root), owing to its chemical purity, very low loss on ignition, high aspect ratio and bright whiteness coupled with its good bioactivity and biocompatibility (De Aza et al., 1999a,b; Kendall, 2001).

---

[*] Corresponding author. Fax: +34 959 219 810.
  E-mail address: caliani@uhu.es (J.C. Fernández-Caliani).

Besides these industrial applications, wollastonite has been effectively tested for the removal of various pollutants from aqueous solutions at the laboratory scale. Panday et al. (1986) reported removal of $Cu^{(II)}$ from aqueous solutions under alkaline conditions, on the basis of the uptake of hydrolyzed adsorbate species by the active surface sites of adsorbent; Yadava et al. (1991) argued that the removal of $Pb^{(II)}$ by adsorption on wollastonite is an attractive process that is highly dependent on the temperature of the adsorbate solution; and Sharma (2003) and Sharma et al. (2007) successfully used wollastonite for the treatment of wastewater and industrial effluents rich in $Cr^{(VI)}$. Recent studies (Likens et al., 2004; Peters et al., 2004) have also documented that the addition of powdered and pelletized wollastonite to a stream affected by acid deposition contributes to the amelioration of the stream-water acidity, concluding that wollastonite may be useful for restoration of aquatic ecosystems that have been anthropogenically acidified.

Wollastonite has dissolution rates under acidic conditions that are comparable with the oxidation rates of pyrite, thereby it can be regarded as significant in terms of having potential to neutralize acidity (Paktunc, 1999; Jambor et al., 2002). Accordingly, the use of wollastonite might be a promising alternative to traditional liming agents to reduce the environmental effects arising from acid mine drainage (AMD) in those regions where there is availability in large quantities at low cost. AMD refers to acid sulfate waters resulting from oxidative dissolution of sulfide minerals (particularly pyrite) exposed in waste-rock piles and tailings impoundments, as a consequence of mining and smelting activities. The general process has been described as follows (Singer and Stumm, 1970):

$$2FeS_2 + 7O_2 + 2H_2O \rightarrow 2Fe^{2+} + 4SO_4^{2-} + 4H^+ \tag{1}$$

$$4Fe^{2+} + O_2 + 4H^+ \rightarrow 4Fe^{3+} + 2H_2O \tag{2}$$

$$4Fe^{3+} + 12H_2O \rightarrow 4Fe(OH)_3 + 12H^+ \tag{3}$$

$$FeS_2 + 14Fe^{3+} + 8H_2O \rightarrow 15Fe^{2+} + 2SO_4^{2-} + 16H^+ \tag{4}$$

Environmental acidification with AMD differs from that caused by acid rain because of extremely low pH, and high concentrations of Fe, Al, other metals, SO_4 and metalloids (Dubikova et al., 2002). AMD is a common problem all over the world and annually millions of litres of heavily con-taminated acid waters are generated. Research on effective and inexpensive methods of treating the AMD is, therefore, of great interest.

This paper presents the results of a series of laboratory experiments on the interaction between wollastonite and acid mine water, which is used as a natural reagent. This approach offers the advantage (over the generally used synthetic solutions prepared from standards) of providing insight on processes occurring in natural systems. The experimental simulation was carried out to evaluate the suitability of wollastonite for AMD remediation by examining the processes that cause its destruction and subsequent effects on water acidity neutralization and removal of metals and metalloids.

2. Material and methods

Reddish water emanating from pyrite-rich wastes around the abandoned mines of Tharsis, SW Spain, in the Iberian Pyrite Belt (IPB), was used as a natural reagent solution for wollastonite dissolution. The IPB comprises more than 80 AMD-generating mine sites, including historic districts like Río Tinto, and represents one of the largest accumulations of pyritic mine wastes in the world (Sánchez-España et al., 2005).

A water sample ($\approx$1 L) of the AMD discharge was taken with a polyethylene bottle and filtered through a 0.45 μm membrane within 24 h of its collection for chemical analysis. Some parameters of the mine water such as pH, Eh, electrical conductivity and temperature were measured *in situ* with portable CRISON instruments.

A representative sample ($\approx$1 kg) of massive wollastonite was selected as a starting material for these experiments. The sample was collected in the Aroche skarn deposit, near the mining district of Tharsis, where a drill-indicated reserve has been outlined of 5.7 million tonnes of mineral (Griffo and Rincón, 1990). The wollastonite sample was white, with a coarse-bladed habit, and individual subidioblastic crystals reaching several centimetres in length.

The wollastonite sample was crushed to a mean grain size of 5 mm and hand sorted to obtain nearly pure wollastonite crystals. About 10 g of the crushed material was ground in an agate mortar, dry-sieved to recover the less than 63 μm grain-size powder, and then split into 4 subsamples. For each of the 4 subsamples, 1 g dry weight was treated with 25 mL of the mine water in polyethylene centrifuge

tubes, at room temperature. The tubes were continuously stirred on an orbital shaker rotating at 12 rpm, thus allowing full contact between the solid particles and the aqueous solution for different lengths of time (15, 30, 50 and 80 days). At the conclusion of each experiment, the pH and electrical conductivity values of the reacted wollastonite suspensions were measured using calibrated electrodes (CRISON). The residual solids were removed by filtration, air dried, and subsequently analysed using a combination of instrumental techniques.

The specific surface area of both the initial wollastonite particles and the solid reaction products was determined by a 3-point BET method, using a N_2 gas adsorption system with a Micromeritics Gemini V Series 2365 apparatus.

Mineralogical analyses of the starting material and the final reaction products were performed by powder X-ray diffraction (XRD) techniques on a BRUKER D8-Advance diffractometer, using monochromatic Cu Kα radiation at 40 kV and 30 mA. The samples were scanned from 3° to 65° 2θ at 0.5 s counting time per step.

The samples were also examined on a JEOL JSM-5410 scanning electron microscope (SEM) by means of secondary electron imaging and energy dispersive system (EDS) for microanalysis (link ISIS system) to determine the morphologies and phase composition of individual particles, operating with an accelerating voltage of 20 kV.

Chemical analyses of the solid samples were undertaken at Activation Laboratories Ltd. (Ontario, Canada) by inductively coupled plasma-optical emission spectrometry (ICP-OES), after a lithium metaborate/tetraborate fusion technique that ensures the entire sample dissolution. Total concentrations of major elements and a suite of trace elements that commonly occur in AMD systems, such as (detection limits between brackets) As ($0.1 mgL^{-1}$), Cd (0.1), Cr (0.5), Co (0.1), Cu (0.2), Ni (0.5) and Pb (0.5) were analysed on a Thermo Jarrell Ash ENVIRO II spectrometer. Quality control included the use of a method reagent blank, several certified reference materials (GRX-1, GRX-2, GRX-4 and GRX-6), and replicates to check accuracy and precision of the analytical data.

The chemical analyses of the acid mine water were performed at the Central Research Services at Huelva University (Spain). The major cations were determined by ICP-OES on a Jobin Yvon ULTIMA 2 spectrometer, following a custom-designed proto-col (Ruiz et al., 2003) contrasted with international reference samples (SRM-1640, IRMM-N3). The trace element concentrations were analysed by inductively coupled plasma-mass spectrometry (ICP-MS) on a Hewlett Packard 4500 instrument, with detection limits of $0.01 \mu gL^{-1}$. The average precision and accuracy fall in the range of 5–10% relative, and they were controlled by repeated analyses of SARM-1 (granite) and SARM-4 (norite) international rock standards.

Equilibrium geochemical speciation/mass transfer model PHREEQC (Parkhurst and Appelo, 2005) with the database of the speciation model MINTEQ (Allison et al., 1991) was applied to determine mineral saturation indices [SI = log(IAP/K$_S$), where SI is the saturation index, IAP is the ion activity product and K$_S$ is the solid solubility product]. Zero, negative and positive SI values indicate that the solutions are saturated, undersaturated and supersaturated, respectively, with respect to a solid phase. For a state of supersaturation, precipitation of the solid phase is expected.

3. Results and discussion

A compilation of pH and electrical conductivity (EC) values, BET surface areas and chemical composition of the starting materials and the solid reaction products obtained in the course of the experiments is given in Table 1.

3.1. Characterization of the starting materials

The wollastonite powder used in this study displayed a XRD pattern indicative of wollastonite-Tc (Fig. 1A), which is referred to as the low-temperature triclinic form. All experiments were run using finely ground wollastonite powder (<63 μm) with a mean BET surface area of $1.19 m^2 g^{-1}$. SEM observations (Fig. 2A) revealed discrete acicular-shape particles with a moderate aspect ratio.

When wollastonite powder was added to distilled water in a solid/liquid ratio of 1:2.5, the pH of the suspension increased to 10.4 in a few minutes, thereby reflecting its alkaline nature. The pH increase results from the release of Ca^{2+} ions into the solution and adsorption of H^+ to the mineral surface (Rimstidt and Dove, 1986; Xie and Walther, 1994). The electrical conductivity of the same wollastonite suspension was found to be $0.4 mS cm^{-1}$. Although fairly close in composition to $CaSiO_3$,

Table 1
Compilation of pH and electrical conductivity (EC) values, BET surface areas and chemical composition of the starting materials and solid reaction products of the dissolution experiments

	Starting materials		Solid reaction products			
	Wollastonite	Acid mine water	15 days	30 days	50 days	80 days
pH	10.4	2.1	3.5	3.6	3.6	3.5
EC (mS cm^{-1})	0.4	15.3	9.2	8.6	8.7	8.7
Surface area (m^2 g^{-1})	1.19	–	30.0	43.3	42.8	47.6
Major elements (%)						
Al	0.17	0.31 (0.46)	3.94	4.24	3.81	3.61
Ca	28.5	0.03 (1.01)	14.8	15.9	16.1	17.3
Fe	0.33	0.14 (1.31)	4.46	4.43	4.05	4.23
K	0.15	0.2 (2.69)	0.04	0.03	0.03	0.02
Mg	0.08	0.18 (4.38)	0.06	0.07	0.06	0.06
Mn	0.07	0.02 (1.09)	0.01	0.01	0.01	0.01
Na	0.011	0.001 (5.41)	0.003	0.003	0.003	0.003
Si	na	0.001 (1.52)	na	na	na	na
S	na	0.8 (3.18)	na	na	na	na
Trace elements (ppm)						
As	bdl	na	49.8	47.3	44.4	46.2
Cd	0.5	1.7 (0.78)	0.2	0.2	0.2	0.2
Co	0.6	325 (0.81)	5.5	7.5	6.4	6.9
Cr	2.5	12.4 (0.40)	14.8	12.1	13.0	14.7
Cu	0.8	4350 (0.74)	477	586	551	566
Ni	14.3	47 (0.87)	8.7	9.7	10.3	10.1
Pb	7.7	bdl	2.6	2.4	2.0	1.9
Zn	17.7	2380 (0.77)	51.6	70.1	63.1	68.8

Relative standard deviation (%) of the results of chemical analysis for each set of triplicate water samples is reported in brackets.
bdl: below detection limit; na: not analyzed.

the starting wollastonite contains appreciable amounts of Fe, Al, K, Mg, Mn, Na, in this order of abundance, and a variety of trace elements in negligible concentrations.

The mine water sample shows the typical hydrogeochemical facies of AMD recognized in the area (e.g., Sánchez-España et al., 2005). It is characterized by a very acidic pH (2.1), relatively high redox potential (Eh = 610 mV) and electrical conductivity (15.3 mS cm^{-1}), and extremely high levels of SO$_4$ (24,100 mg L^{-1}) and certain heavy metals, such as Cu (4350 mg L^{-1}) and Zn (2380 mg L^{-1}).

3.2. Characterization of the reaction products

The mineralogical analysis by XRD of the reaction products (Fig. 1B) showed that gypsum (CaSO$_4$ · 2H$_2$O) is the only crystalline phase formed during the long-term interaction of wollastonite with acid mine water, regardless of contact time. It is assumed, therefore, that the rest of the solids found in the residual material correspond to amorphous or poorly crystalline phases. SEM observa-

tions (Fig. 2B) confirmed the appearance of neoformed gypsum crystals up to 100 μm long that invariably occur as single euhedral crystals with well-developed {0 1 0} forms. A rough estimation from the SEM photomicrographs indicates that the abundance of gypsum increased from 15% to 20% upon treatment.

The reacted wollastonite crystals preserved their original prismatic morphology, although they exhibit apparently cracked warty surfaces (Fig. 2C). A more detailed examination of the crystal surfaces revealed that the reacted wollastonite appears to be encapsulated by a thin coating (<1 μm thickness) of microbotryoidal masses of amorphous phases chemically composed of Al, Fe, S and minor Ca and Cu, as detected by EDS (Fig. 2D). These coatings are similar in both appearance and composition to amorphous Fe–Al oxy-hydroxides and oxy-hydroxysulfates that are often found on armoured calcite grains when acid solutions are neutralized with limestone (Al et al., 2000; Hammarstrom et al., 2003; Simon et al., 2005). The rust-colored stains on the reacted sample after treatments, in con-
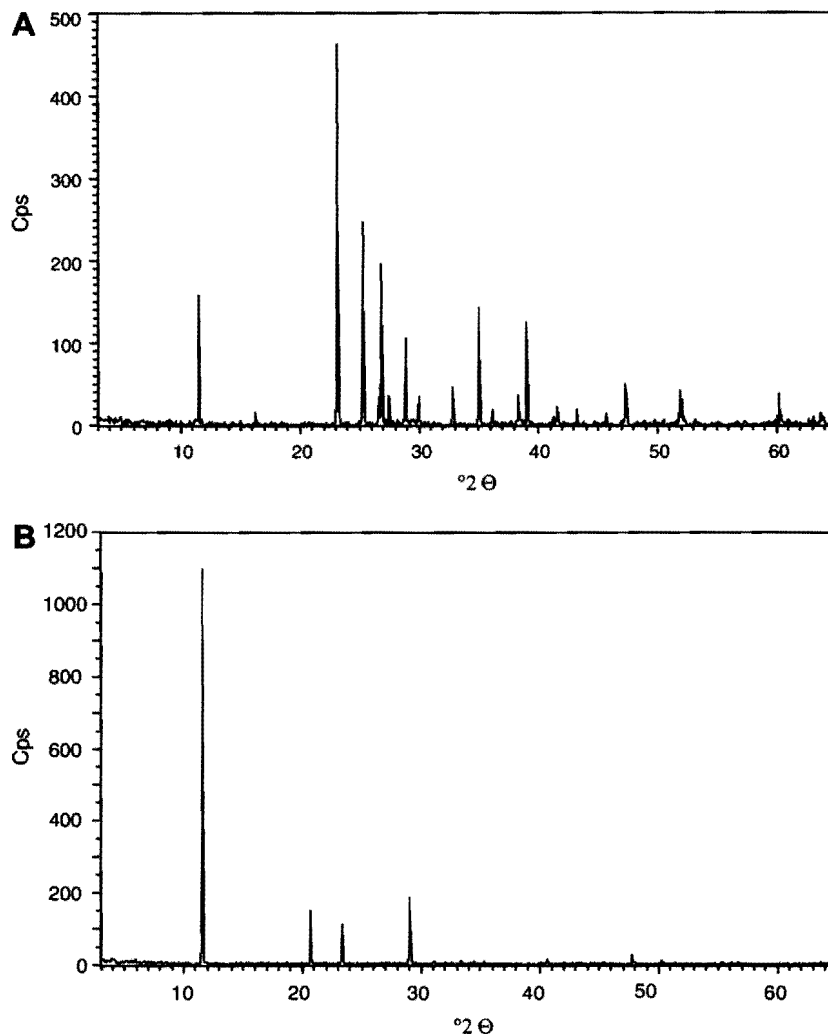
Fig. 1. XRD diffractograms of the untreated wollastonite powder used as starting material (A) and the crystalline reaction product (gypsum) obtained after 15 days of acid treatment (B).

trast to the whiteness of the starting wollastonite, also suggest the occurrence of Fe-rich secondary phases.

The armour coatings developed a network of open microcracks because of shrinkage induced by desiccation of the reacted sample, exposing sections of the underlying substrate as shown in Fig. 2D. The EDS spectra show that the substrate is composed essentially of pure silica, thus providing evidence for amorphous silica pseudomorphism after wollastonite. In many cases, the armour has partially scaled off along the cracks forming detached globular or spherulitic aggregates that display EDS analytical results similar to those of the coatings (Fig. 2E and F).

3.3. Solid-fluid interaction and effects on metal removal

It has long been known that wollastonite reacts readily with acid solutions. The hydrolysis of wollastonite in an acid environment may be described by the following reaction (Murphy and Helgeson, 1987):

$$CaSiO_3 + 2H^+ \rightarrow Ca^{2+} + H_2SiO_3 \qquad (5)$$
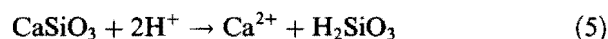
Accordingly, dissolution of wollastonite driven by acid mine drainage is consistent with an effective exchange reaction, in which Ca^{2+} is exchanged with adsorbed H^+ and diffused out of the crystal structure into the solution, leaving a residual
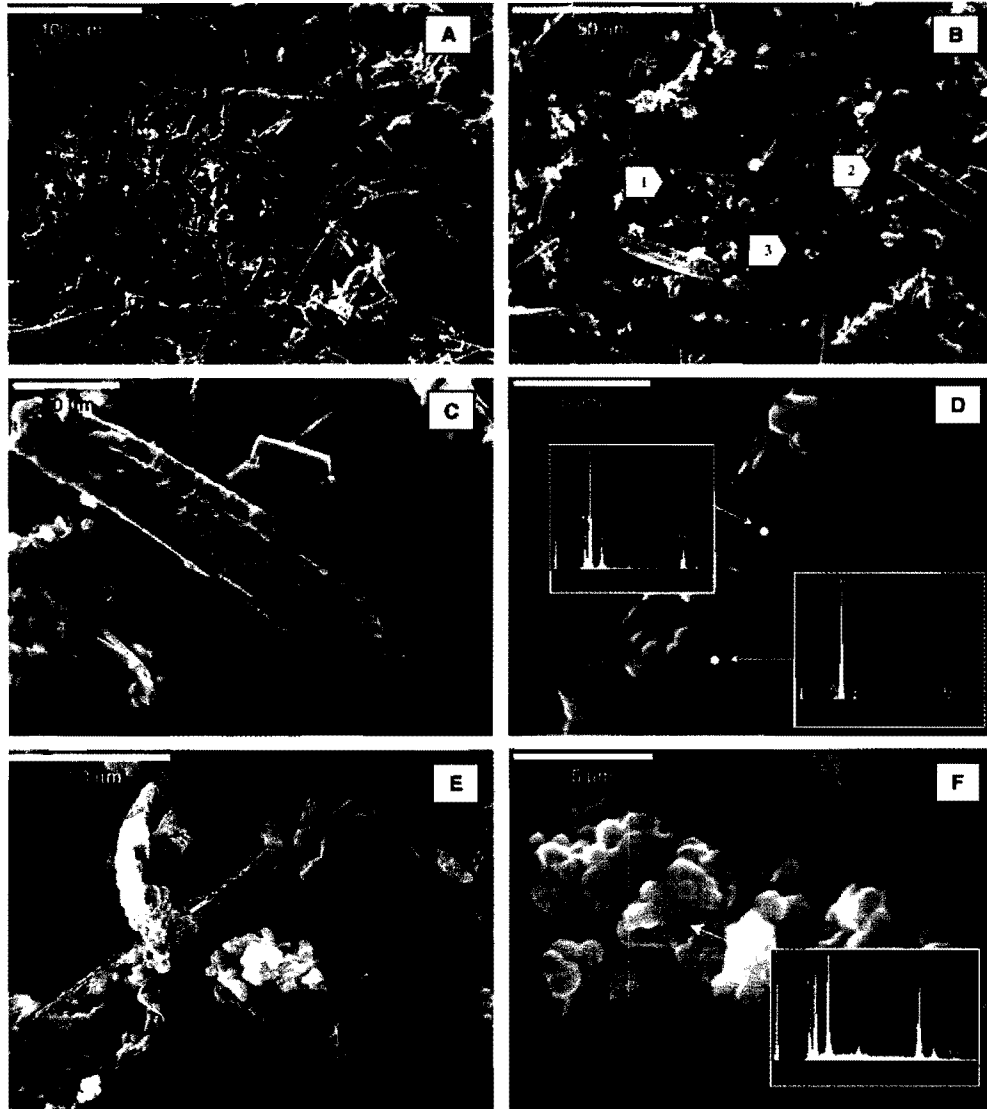
Fig. 2. SEM photomicrographs showing: (A) pristine crystals of wollastonite before interaction with AMD; (B) reaction products of wollastonite dissolution after 15 days of treatment (1: reacted-wollastonite; 2: gypsum crystal; and 3: aggregates of newly formed amorphous phases); (C) armour coating developed on the reacted-wollastonite surface; (D) a detail of the cracked coating surface, and EDS spectra of the new solid silica pseudomorph after wollastonite and the coating; (E) spherulitic aggregates of amorphous phases scaled off along the cracks of the coating; and (F) a high-magnification image and EDS spectrum of the sphere-like colloidal-size particles.

amorphous phase that exhibits the morphology of the parent wollastonite crystals. It can be assumed, therefore, that wollastonite dissolved incongruently, with a greater release of weakly bound Ca than covalently bonded Si relative to the wollastonite stoichiometry. Unfortunately, in this acidic system the physicochemical conditions are not well-fixed, and so the fluid composition cannot be easily interpreted in terms of simple thermodynamic diagrams.

Based on atomistic simulation techniques, Kundu et al. (2003a,b) documented that preferential release of Ca^{2+} is energetically favourable under acidic conditions. The more rapid release of Ca relative to Si in the early stage of reaction progress must have formed a silica-rich leached layer on the surface of the dissolving wollastonite, whose average thickness is a function of both H^+ activity and time (Weissbart, 1997; Weissbart and Rimstidt, 2000). Measurements of dissolution rates in acid

solutions are independent of pH and range from 6.03×10^{-9} to 12.1×10^{-9} mol Ca m^{-2} s^{-1} according to Weissbart and Rimstidt (2000).

The presence of completely Ca-free solid pseudomorphs after wollastonite suggests that, under the strong acidic conditions and long term solid-fluid interaction of the experiments, virtually all the Ca was removed from the crystal structure through the leached layer. This assertion is also supported by the fact that a wollastonite diffraction pattern is absent in the XRD diagrams of the reaction products. The complete removal of Ca probably happened before armouring took place, as the armour coatings could have acted as a barrier hindering Ca transport into solution. Although some Si could have been released by Si–O–Si bond hydrolysis, the residual silica must have restructured into a newly developed amorphous phase. Silica reconstruction into a less reactive form resembling vitreous silica has been inferred by spectroscopic studies dealing with acid-leached wollastonite (Casey et al., 1993; Schott et al., 2002).

The specific surface area of the reacted wollastonite is 40 times greater than that of the starting wollastonite. The mean BET surface area of the reaction products increased from an initial value of 1.19 m^2 g^{-1} to as high as 30 m^2 g^{-1} after 15 days of reaction with the acid mine water, and it increased over time to 47.6 m^2 g^{-1}. The largest increase in surface area occurred at the beginning of treatment, probably because of the formation of large etch pits and disaggregation of the wollastonite crystals with a consequent reduction of grain size (Rimstidt and Dove, 1986; Xie and Walther, 1994). In addition, the formation of poorly crystallized Fe–Al oxy-hydroxides and oxy-hydroxysulfates would also contribute to the increased surface area (Bigham et al., 1990).

The dissolution reaction of wollastonite consumes acidity owing to readily available Ca^{2+} ions. In theory, 1 mol wollastonite has the potential to neutralize 2 mol H_2SO_4, assuming complete dissolution without precipitation of secondary phases. The release of Ca^{2+} into solution resulted in a pH increase from 2.1 to 3.5, and it had a buffering action because the pH of the reacted wollastonite suspensions remained almost constant over time.

The occurrence of gypsum in the reaction products of the wollastonite dissolution can be easily explained by precipitation of the Ca-saturated SO_4 solution. Most of the Ca^{2+} ions released from the wollastonite into solution reacted with the acid sulphate water through the following reaction:

$$Ca^{2+} + SO_4^{2-} + 2H_2O \rightarrow CaSO_4 \cdot 2H_2O \qquad (6)$$
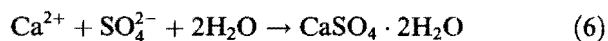
The precipitation of gypsum partly affected the electrical conductivity of the solution, which dropped from 15.3 to 9.2 mS cm^{-1} within the first 15 days of treatment, and subsequently remained relatively constant at about 8.6–8.7 mS cm^{-1}.

The concentration of Ca in the products obtained after 15 days reaction time was 14.8%, and increased to 17.3% upon treatment for 80 days due to progressive precipitation of gypsum. Therefore, a range between 51.9% and 60.7% of the Ca released by wollastonite dissolution seems to be retained in the residual material. Despite this result, the reaction products appear clearly depleted in Ca relative to the starting wollastonite because a significant amount of Ca^{2+} ions were leached, together with traces of other alkaline and alkaline-earth elements.

In contrast, the amorphous residual material is largely enriched in elements commonly associated with AMD, such as Fe (4.01–4.46%) and Al (3.61–4.24%), as result of removal from the acid mine water. In fact, when the dissolving wollastonite raised the pH, much of the $Fe^{(III)}$ ions precipitated on grain surfaces developing a secondary-mineral coating of amorphous or nanocrystalline Fe oxy-hydroxides and/or oxy-hydroxysulfates, as shown by SEM-EDS and by the lack of diffraction effects in the XRD diagrams. The high relative content of Al in the coating may result from both precipitation of Al oxy-hydroxides and/or oxy-hydroxysulfates and coprecipitation with Fe oxy-hydroxides, as previously observed by Gerth (1990), because of its low solubility even at low pH values. The Ca content of the coating is presumably in the form of gypsum.

Thermodynamic calculations predicted supersaturation in the observed phases. After reaction, the PHREEQC modeling code indicates that the solutions are supersaturated with respect to gypsum, amorphous silica and Fe–Al oxy-hydroxides and/or oxy-hydroxysulfates (Table 2), consistent with the evidence of the precipitation and presence of these phases in the reaction products. Iron oxy-hydroxides and/or oxy-hydroxysulfates correspond to minerals of the jarosite group, schwertmannite, ferrihydrite and goethite. Although solutions are theoretically supersaturated in these Fe-rich minerals, schwertmannite appears to be the most stable phase thermodynamically, as shown in the

Table 2
Ideal reactions, equilibrium constants ($\log K_{eq}$) and saturation indices (SI) for supersaturated minerals resulting from wollastonite–AMD interaction

Mineral	Reaction	Log K_{eq}	SI
Alunite	$KAl_3(SO_4)_2(OH)_6 + 6H^+ \Leftrightarrow K^+ + 3Al^{+3} + 2SO_4^{-2} + 6H_2O$	−1.346	5.14
Amorphous SiO_2	$SiO_2(am) + 2H_2O \Leftrightarrow H_4SiO_4$	−2.71	0.7
Basaluminite	$Al_4(OH)_{10}SO_4 + 10H^+ \Leftrightarrow 4Al^{+3} + SO_4^{-2} + 10H_2O$	22.7	0.15
Ferrihydrite	$Fe(OH)_3 + 3H^+ \Leftrightarrow Fe^{+3} + 3H_2O$	4.891	0.15
Goethite	$FeOOH + 3H^+ \Leftrightarrow Fe^{+3} + 2H_2O$	0.5	4.7
Gypsum	$CaSO_4 \cdot 2H_2O \Leftrightarrow Ca^{+2} + SO_4^{-2} + 2H_2O$	−4.848	0.4
Jarosite-K	$KFe_3(SO_4)_2(OH)_6 + 6H^+ \Leftrightarrow K^+ + 3Fe^{+3} + 2SO_4^{-2} + 6H_2O$	−14.8	10.2
Jarosite-Na	$NaFe_3(SO_4)_2(OH)_6 + 6H^+ \Leftrightarrow Na^+ + 3Fe^{+3} + 2SO_4^{-2} + 6H_2O$	−11.2	8.7
Jarosite-H	$(H_3O)Fe_3(SO_4)_2(OH)_6 + 5H^+ \Leftrightarrow 3Fe^{+3} + 2SO_4^{-2} + 7H_2O$	−12.1	9.8
Jurbanite	$AlOHSO_4 + H^+ \Leftrightarrow Al^{+3} + SO_4^{-2} + H_2O$	−3.23	2.2
Schwertmannite[a]	$Fe_8O_8(OH)_{8-2x}(SO_4)_x + (24-2x)H^+ \Leftrightarrow 8Fe^{+3} + xSO_4^{-2} + (16-2x)H_2O$	18 2.5[b]	3.2–8.2
Schwertmannite[a]	$Fe_8O_8(OH)_{8-2x}(SO_4)_x + (24-2x)H^+ \Leftrightarrow 8Fe^{+3} + xSO_4^{-2} + (16-2x)H_2O$	10 2.5[c]	10.7–15.7

All equilibrium constants are from the database of model MINTEQ (Allison et al., 1991), except for schwertmannite.

[a] $x = 1.84$ according to Acero et al., 2006.
[b] Thermodynamic data from Bigham et al., 1996.
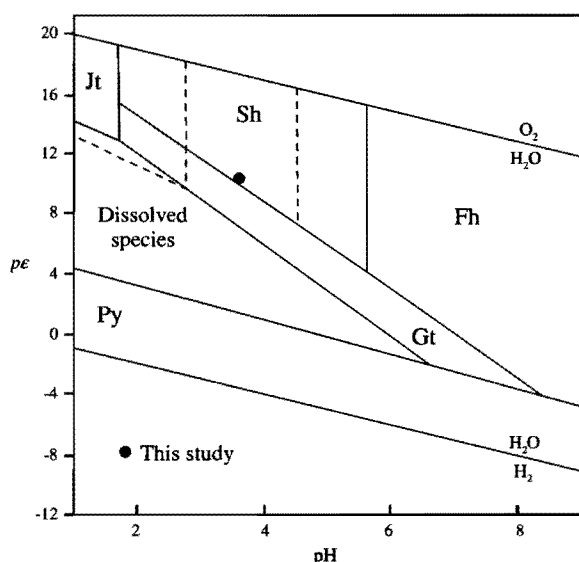[c] Thermodynamic data from Yu et al., 1999.

Fig. 3. Eh and pH projection into the sulphur-iron $p\varepsilon$-pH diagram for the solution resulting from wollastonite–AMD interaction (modified from Bigham et al., 1996). The $p\varepsilon$-pH diagram is for the system Fe–S–K–O–H at 25 °C and 1 bar pressure; assuming $pe = Eh(mv)/59.2$ and total log activities of $Fe^{2+} = -3.47$; $Fe^{3+} = -3.36$ or -2.27; $SO_4^{2-} = -2.32$, $K^+ = -3.78$. Mineral abbreviations: Jt = K-jarosite, Sh = schwertmannite, Fh = ferrihydrite, Gt = goethite, Py = pyrite. Darker areas show possible expansion of K-jarosite and ferrihydrite fields.

sulphur–iron $p\varepsilon$-pH stability diagram (Fig. 3), as well as the most important mineral controlling the Fe solubility. On the other hand, Al solubility seems to be controlled by a mixture of amorphous or poorly crystallized phases like alunite, jurbanite and basaluminite.

In terms of trace elements, the coatings show relatively high concentrations of As (up to 49.8 ppm) and certain metals like Cu (up to 586 ppm), Zn (up to 68.8 ppm), Cr (up to 14.8 ppm) and Co (up to 7.5 ppm) when compared to the starting wollastonite. Fig. 4 depicts the total concentrations of these trace elements retained in the residual material for each reaction time interval. The rate of removal was rapid in early stages and became nearly constant when equilibrium was attained, as indicated by the slope of the plots.

The enrichment was particularly remarkable for As and Cu, whose enrichment factors are greater than 500 relative to wollastonite. Nonetheless, the concentration of potential pollutants retained in the reaction products is discrete regarding the metal load dissolved in the AMD solution because not enough alkaline material was used to remediate the acidity of the system, and consequently to reduce the mobility of metals. The extent of removal from the solution, at a pH of between 2.1 and 3.5, seems to depend on the nature and concentration of metals in the solution. Thus, for instance, the percentage of Cu sequestered in the residual material ranges from 11% to 13.5%, whereas almost all the Cr was removed upon treatment.

Theoretically, the Fe oxy-hydroxides and oxy-hydroxysulfates may have effectively removed the trace elements dissolved in the AMD solution by means of adsorption and coprecipitation, as previously described in a number of papers (e.g., Benjamin and Lecki, 1981; Bigham et al., 1996; Cravotta and Trahan, 1999). At such low pH
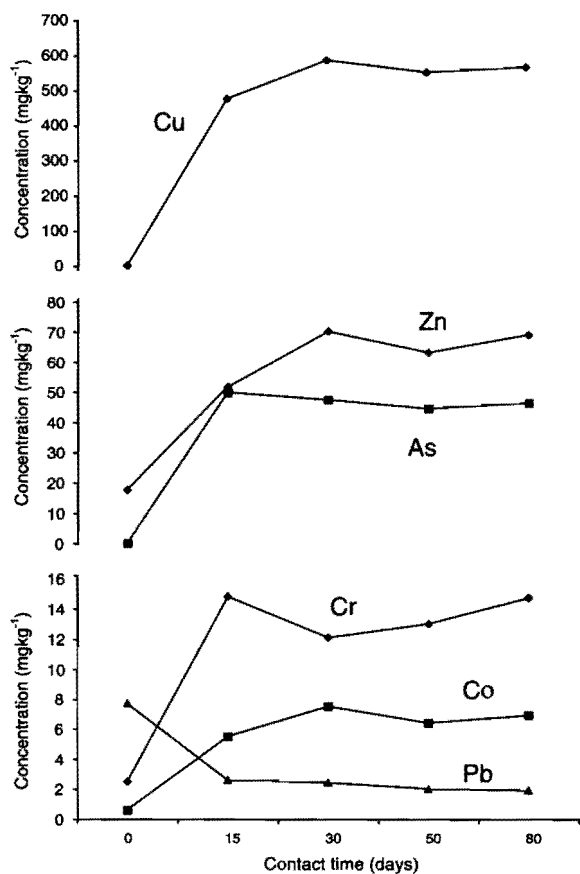
Fig. 4. Trace element concentrations (in mg kg^{-1}) in the solid reaction products of wollastonite dissolution with acid mine water as a function of contact time (in days).

Fig. 5. Representation of pH and log (a_{Fe}^{+3}) vs. wollastonite amount. Simulation performed with PHREEQC considering acid mine waters in equilibrium with different amounts of wollastonite. Vertical line represents conditions of the experiment.

values, adsorption was apparently the most efficient immobilization mechanism for oxyanions (As and Cr), and consequently for the attenuation of their concentrations in the aqueous solution. Sharma (2003) found maximum removal of Cr$^{(VI)}$ by wollastonite at a pH around 2.5 because of a significantly high electrostatic attraction between adsorbent and adsorbate. However, the percentage of metals adsorbed by the reaction products of the wollastonite dissolution was of minor importance due to, in large part, the competition of H$^+$ ions and metal cations for binding sites. The uptake of cations by the acid-reacted wollastonite generally occurs between pH 7 and 10 (Panday et al., 1986; Xie and Walther, 1994) suggesting that cation adsorption at the wollastonite/water interface is important only in alkaline aquatic environments. Therefore, coprecipitation with Fe oxy-hydroxides and oxy-hydroxysulfates is the mechanism that represents the most likely explanation for the increased abun-
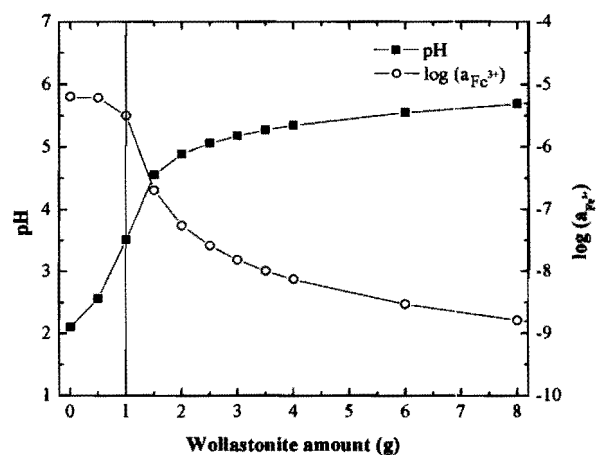
dance of metals (especially Cu) in the coatings. No formation of any discrete Cu and Zn-bearing minerals was predicted through geochemical modeling.

On the other hand, the reaction products show contents of Pb and Ni lower than those of the starting material. Taking into account that the abundance of Pb dissolved in the acid water is negligible (<0.01%), it can be assumed that virtually all Pb retained in the residual material (2.6 ppm after 15 days of treatment) derived from the wollastonite breakdown. The concentration of this metal in the reaction products gradually decreases over time up to 1.9 ppm, suggesting that a labile fraction was leached to some extent during the solid–water interaction. Conversely, the amount of Ni retained in the reacted sample tended to increase upon treatment, although most of this metal remained in solution.

The secondary Fe minerals not only control the metal solubility but also the pH of the AMD solution. The protons released by Fe$^{(III)}$ precipitation nearly buffers the increase in alkalinity derived from wollastonite dissolution, keeping the pH value around 3.5. However, by doubling the wollastonite amount in the system, the pH would increase to about 5, and then dissolved Fe$^{(III)}$ activity in solution would decrease noticeably (Fig. 5), resulting in more effective metal retention.

4. Conclusions

In this study, experiments were conducted in which wollastonite was reacted with acid mine

drainage at a mass ratio of 1:25. The results suggest that wollastonite was incongruently dissolved after long-term reaction with the AMD solution and pseudomorphically replaced by a coated amorphous silica-rich phase, thus increasing significantly the specific surface area of the residual material. The release of Ca into solution resulted in a pH increase from 2.1 to 3.5, and subsequent precipitation of gypsum took place from the Ca-saturated sulphate solution along with a mixture of amorphous or poorly crystalline Fe–Al oxyhydroxides and oxy-hydroxysulfates, which constitute the coating. Geochemical modeling with PHREEQC indicates that schwertmannite, goethite and minerals of the jarosite group play a significant role in controlling the Fe solubility after wollastonite–AMD interaction, while the Al solubility appears to be controlled mainly by alunite, jurbanite and basaluminite. The formation of the armour coating promoted the removal of a variable fraction of trace elements dissolved in the AMD solution, especially As, Cr, Cu and Zn, as indicated by their enrichment relative to the parent wollastonite. The dominant mechanisms of immobilization at such low pH values probably were adsorption of As and Cr oxyanions on the positively charged solid particles, and metal coprecipitation (mainly Cu and Zn) with the amorphous Fe oxy-hydroxides and/or oxy-hydroxysulfates. Nevertheless, further research is required to examine in more detail the factors controlling the removal and partitioning of metals and metalloids.

Finally, although wollastonite would not be a low cost agent to remediate the environmental effects of AMD in general, it might be a useful first stage in attenuation of acidity and metal contamination, particularly in the Iberian Pyrite Belt and other historically heavily contaminated areas where there is a nearby source of nearly pure mineral.

Acknowledgements

The authors wish to thank Richard Wanty and Wilson Gitari for their constructive reviews and helpful comments that greatly improved the manuscript.

References

Acero, P., Ayora, C., Torrentó, C., Nieto, J.M., 2006. The behaviour of trace elements during schwertmannite precipitation and subsequent transformation into goethite and jarosite. Geochim. Cosmochim. Acta 70, 4130–4139.

Al, T.A., Martin, C.J., Blowes, D.W., 2000. Carbonate-mineral/water interactions in sulfide-rich mine tailings. Geochim. Cosmochim. Acta 64, 3933–3948.
Allison, J.D., Brown, D.S., Novo-Gradac, K.J., 1991. MINTEQA2/PRODEFA2, A geochemical assessment model for environmental systems, Version 3.0 User's Manual, Environmental Research Laboratory, Office of Research and Development, US Environmental Protection Agency, EPA/600/3-91/021, Athens, Georgia, 30605.
Benjamin, M.M., Lecki, J.O., 1981. Multiple-site adsorption of Cd, Cu, Zn and Pb on amorphous iron oxyhydroxides. J. Colloid Interf. Sci. 79, 209–221.
Bigham, J.M., Schwertmann, U., Carlson, L., Murad, E., 1990. A poorly crystallized oxyhydroxysulfate of iron formed by bacterial oxidation of Fe(II) in acid mine waters. Geochim. Cosmochim. Acta 54, 2743–2758.
Bigham, J.M., Schwertmann, U., Traina, S.J., Winland, R.L., Wilf, M., 1996. Schwertmannite and the chemical modeling of iron in acid sulfate waters. Geochim. Cosmochim. Acta 60, 2111–2121.
Casey, W.H., Westrich, H.R., Banfield, J.F., Ferruzzi, G., Arnold, G.W., 1993. Leaching and reconstruction at the surfaces of dissolving chain-silicate minerals. Nature 366, 253–256.
Cravotta, C.A., Trahan, M.K., 1999. Limestone drains to increase pH and remove dissolved metals from acidic mine drainage. Appl. Geochem. 14, 581–606.
De Aza, P.N., Luklinska, Z.B., Anseu, M.R., Guitian, F., De Aza, S., 1999a. Bioactivity of pseudowollastonite in human saliva. J. Dent. 27, 107–113.
De Aza, P.N., Luklinska, Z.B., Martínez, A., Anseu, M.R., Guitian, F., De Aza, S., 1999b. Morphological and structural study of pseudowollastonite implants in bone. J. Microsc. 197, 60–67.
Dubikova, M., Cambier, P., Sucha, V., Caplovicova, M., 2002. Experimental soil acidification. Appl. Geochem. 17, 245–257.
Fernández-Caliani, J.C., Galán, E., 1998. Effects of fluid infiltration on wollastonite genesis at the Mérida contact-metamorphic deposits, SW Spain. Mineral. Petrol. 62, 247–267.
Gerdes, M.L., Valley, J.W., 1994. Fluid flow and mass transport at the Valentine wollastonite deposit, Adirondack Mountains, New York State. J. Metamorph. Geol. 12, 589–608.
Gerth, J., 1990. Unit-cell dimensions of pure and trace-metal associated goethites. Geochim. Cosmochim. Acta 54, 363–371.
Grammatikopoulos, T.A., Clark, A.H., 2006. A comparative study of wollastonite skarn genesis in the Central Metasedimentary Belt, southeastern Ontario, Canada. Ore Geol. Rev. 29, 146–161.
Griffo, J.L., Rincón, A., 1990. El yacimiento de wollastonita de Aroche (Huelva). Canteras y Explotaciones 280, 95–108.
Hammarstrom, J.M., Sibrell, P.L., Belkin, H.E., 2003. Characterization of limestone reacted with acid-mine drainage in a pulsed limestone bed treatment system at the Friendship Hill National Historical Site, Pennsylvania, USA. Appl. Geochem. 18, 1705–1721.
Jambor, J.L., Dutrizac, J.E., Groat, L.A., Raudsepp, M., 2002. Static test of neutralization potentials of silicate and aluminosilicate minerals. Environ. Geol. 43, 1–17.
Kendall, T., 2001. Wollastonite review. Ind. Miner. 411, 63–67.
Kundu, T.K., Hanumantha Rao, K., Parker, S.C., 2003a. Atomistic simulation of the surface structure of wollastonite. Chem. Phys. Lett. 377, 81–92.

Kundu, T.K., Hanumantha Rao, K., Parker, S.C., 2003b. Atomistic simulation of the surface structure of wollastonite and adsorption phenomena relevant to flotation. Int. J. Miner. Process. 72, 111–127.

Likens, G.E., Buso, D.C., Dresser, B.K., Bernhardt, E.S., Hall, R.O., Macneale, K.H., Bailey, S.W., 2004. Buffering an acidic stream in New Hampshire with a silicate mineral. Restor. Ecol. 12, 419–428.

Murphy, W.M., Helgeson, H.C., 1987. Thermodynamic and kinetic constraints on reaction rates among minerals and aqueous solutions. III. Activated complexes and the pH-dependence of the rates of feldspar, pyroxene, wollastonite, and olivine hydrolysis. Geochim. Cosmochim. Acta 51, 3137–3153.

Paktunc, A.D., 1999. Characterization of mine wastes for prediction of acid mine drainage. In: Azcue, J.M. (Ed.), Environmental Impacts of Mining Activities. Springer, Berlin, pp. 9–40.

Panday, K.K., Prasad, G., Singh, V.N., 1986. Use of wollastonite for the treatment of Cu(II) rich effluents. Water Air Soil Pollut. 27, 287–296.

Parkhurst, D.L., Appelo, C.A.J., 2005. PHREEQC-2 version 2.12: A hydrochemical transport model. <http://wwwbrr.cr.usgs.gov>.

Peters, S.C., Blum, J.D., Driscoll, C.T., Likens, G.E., 2004. Dissolution of wollastonite during the experimental manipulation of Hubbard Brook Watershed 1. Biogeochemistry 67, 309–329.

Rimstidt, J.D., Dove, P.M., 1986. Mineral/solution reaction rates in a mixed flow reactor: Wollastonite hydrolysis. Geochim. Cosmochim. Acta 50, 2509–2516.

Ruiz, M.J., Carrasco, R., Pérez, R., Sarmiento, A.M., Nieto, J.M., 2003. Optimización del análisis de elementos mayores y traza mediante ICP-OES en muestras de drenaje ácido de mina. In: Proceedings of IV Iberian Geochemical Meeting, University of Coimbra (Portugal), pp. 402–404.

Sánchez-España, J., López-Pamo, E., Santofimia, E., Aduvire, O., Reyes, J., Barettino, D., 2005. Acid mine drainage in the Iberian Pyrite Belt (Odiel river watershed, Huelva, SW, Spain): Geochemistry, mineralogy and environmental implications. Appl. Geochem. 20, 1320–1356.

Schott, J., Pokrovsky, O.S., Spalla, O., Devreux, F., Mielczarski, J.A., 2002. The mechanism of altered layers formation on wollastonite revisited: a combined spectroscopic/kinetic study. Geochim. Cosmochim. Acta 66 (15A, Suppl. 1), A-686 (Goldschmidt Conf. Abst.).

Sharma, Y.C., 2003. Cr(VI) removal from industrial effluents by adsorption on an indigenous low-cost material. Colloid Surface A 215, 155–162.

Sharma, Y.C., Uma, Srivastava, V., Srivastava, J., Mahto, M., 2007. Reclamation of Cr(VI) rich water and wastewater by wollastonite. Chem. Eng. J. 127, 151–156.

Simon, M., Martín, F., García, I., Bouza, P., Dorronsoro, C., Aguilar, J., 2005. Interaction of limestone grains and acidic solutions from the oxidation of pyrite tailings. Environ. Pollut. 135, 65–72.

Singer, P.C., Stumm, W., 1970. Acid mine drainage: the rate determining step. Science 197, 1121–1123.

Weissbart, E.J., 1997. The leached layer formed on wollastonite in an acid environment. M.Sc. thesis, Virginia Polytechnic Institute and State University.

Weissbart, E.J., Rimstidt, J.D., 2000. Wollastonite: incongruent dissolution and leached layer formation. Geochim. Cosmochim. Acta 64, 4007–4016.

Xie, Z., Walther, J.V., 1994. Dissolution stoichiometry and adsorption of alkali and alkaline earth elements to the acid-reacted wollastonite surface at 25 °C. Geochim. Cosmochim. Acta 58, 2587–2598.

Yadava, K.P., Tyagi, B.S., Singh, V.N., 1991. Effects of temperature on the removal of lead(II) by adsorption on china-clay and wollastonite. J. Chem. Technol. Biotechnol. 51, 47–60.

Yu, J.Y., Heo, B., Choi, I.K., Cho, J.P., Chang, H.W., 1999. Apparent solubilities of schwertmannite and ferrihydrite in natural stream waters polluted by mine drainage. Geochim. Cosmochim. Acta 63, 3407–3416.